Available online at www.sciencedirect.com
SCIENCE DIRECT
Journal of Magnetic Resonance 179 (2006) 241–249
JMR Journal of Magnetic Resonance
www.elsevier.com/locate/jmr

Optimal control design of constant amplitude phase-modulated pulses: Application to calibration-free broadband excitation

Thomas E. Skinner [a,*], Kyryl Kobzar [b], Burkhard Luy [b], M. Robin Bendall [c], Wolfgang Bermel [d], Navin Khaneja [e], Steffen J. Glaser [b]

[a] *Physics Department, Wright State University, Dayton, OH 45435, USA*
[b] *Department of Chemistry, Technische Universität München, Lichtenbergstr. 4, 85747 Garching, Germany*
[c] *Adiabatics, Inc., 83 S. Branciforte, Santa Cruz, CA 95062, USA*
[d] *Bruker BioSpin GmbH, Silberstreifen 4, 76287 Rheinstetten, Germany*
[e] *Division of Engineering and Applied Sciences, Harvard University, 29 Oxford Street, Cambridge, MA 02138, USA*

Received 26 August 2005; revised 5 December 2005
Available online 18 January 2006

Abstract

An optimal control algorithm for generating purely phase-modulated pulses is derived. The methodology is applied to obtain broadband excitation with unprecedented tolerance to RF inhomogeneity. Design criteria were transformation of $I_z \rightarrow I_x$ over resonance offsets of ± 25 kHz for constant RF amplitude anywhere in the range 10–20 kHz, with a pulse length of 1 ms. Simulations transform I_z to greater than 0.99 I_x over the targetted ranges of resonance offset and RF variability. Phase deviations in the final magnetization are less than 2–3° over almost the entire range, with sporadic deviations of 6–9° at a few offsets for the lowest RF (10 kHz) in the optimized range. Experimental performance of the new pulse is in excellent agreement with the simulations, and the robustness of the excitation pulse and a derived refocusing pulse are demonstrated by insertion into conventional HSQC and HMBC-type experiments.

Keywords: BEBOP; Broadband excitation; Optimal control theory; Phase modulation; PM pulses

1. Introduction

Although dual compensation for RF inhomogeneity/miscalibration and chemical-shift offset effects in excitation has been difficult to achieve [1–13], broadband excitation by optimized pulses (BEBOP) [14–17] has been shown to be an effective solution for RF tolerance of 10–15%, which is typical of calibrated pulses output by high-quality RF probes. Broadband in this context refers to a pulse capable of uniformly exciting the entire ^{13}C chemical-shift range at field strengths of 800–900 MHz, requiring a bandwidth of 40–50 kHz.

Broadband pulses which tolerate an even higher degree of RF inhomogeneity could also be useful. NMR-spectroscopy on natural products is one potential application. For example, calibration of ^{13}C-pulses is extremely difficult for natural abundance samples at very low concentration. Moreover, significant variations in pulse length can be caused by varying salt concentrations. Sufficient RF tolerance would remove the need for painstakingly accurate pulse calibrations, which are also important for optimal sensitivity of many complex multidimensional experiments or the automated acquisition of a large number of strongly differing samples.

Encouraged by the success of optimal control theory in designing broadband pulses with outstanding performance, we therefore consider a problem which has been resistant to a successful solution: nearly calibration-free broadband excitation. To accommodate the majority of ^{13}C probes in

* Corresponding author. Fax: +1 937 775 2222.
E-mail addresses: thomas.skinner@wright.edu (T.E. Skinner), glaser@ch.tum.de (S.J. Glaser).

1090-7807/$ - see front matter © 2006 Elsevier Inc. All rights reserved.
doi:10.1016/j.jmr.2005.12.010

use, the pulse should operate equally well for a peak RF output anywhere in the range 10–20 kHz (25–12.5 μs pulse width).

In addition, while the BEBOP pulses obtained to date exhibit nearly ideal performance, their rapid and extreme amplitude jumps can require some monitoring and adjustment of system hardware, primarily with regard to amplifier linearity and accurate output of the waveform generators. We have demonstrated that this is not a problem for modern NMR-consoles with linearized amplifiers and fast amplitude and phase switching times. For NMR-spectrometers equipped with non-linearized amplifiers, however, constant amplitude pulses would be more convenient.

For a given bandwidth and tolerance to RF variability, an optimal control algorithm which allows amplitude/phase modulation and limits the maximum RF amplitude produces a purely phase-modulated pulse when the pulse length is reduced below a certain level [16]—the algorithm pins the RF to its maximum allowed value at all times during the pulse in attempting to optimize pulse performance. For longer pulse lengths, the algorithm is able to converge to a solution using lower, time-variable values of the amplitude without having to consider larger RF values. Instead of reducing pulse length by trial-and-error until constant amplitude pulses are found, it is more efficient to derive them directly, which is the topic of the next section. The results of the new procedure for deriving phase-modulated pulses and their applications in HSQC and HMBC-type experiments are discussed in a following section.

2. Theory and methods

Details of the optimal control procedure, as it relates to broadband excitation in NMR, and the algorithms developed so far are discussed in [14,15,17]. More general information on broadband excitation [1–13], optimal control theory [18–21], and its use in NMR [22–25] can be found in the references. In this section, we derive the modifications to our previous treatment that are required to maximize the performance of a pulse modulated only in phase.

2.1. Optimal control theory: application to excitation

We first provide a synopsis describing those aspects of the methodology that are unaffected by the transition to a phase-modulated pulse. During the time interval $[t_0, t_p]$, we seek to transfer initial magnetization $\boldsymbol{M}(t_0) = \hat{\boldsymbol{z}}$ to the target final state $\boldsymbol{F} = \hat{\boldsymbol{x}}$ for a specified range of chemical-shift offsets and a desired degree of tolerance to RF inhomogeneity or miscalibration. The trajectories $\boldsymbol{M}(t)$ are constrained by the Bloch equation

$$\dot{M} = \boldsymbol{\omega}_e \times M. \tag{1}$$

The effective RF field $\boldsymbol{\omega}_e$ in angular frequency units (rad/s) can be written in the rotating frame as

$$\begin{aligned}\boldsymbol{\omega}_e &= \omega_1(t)[\cos\phi(t)\hat{\boldsymbol{x}} + \sin\phi(t)\hat{\boldsymbol{y}}] + \Delta\omega\hat{\boldsymbol{z}} \\ &= \boldsymbol{\omega}_{\mathrm{rf}}(t) + \Delta\omega\hat{\boldsymbol{z}},\end{aligned} \tag{2}$$

which encompasses any desired modulation of the amplitude ω_1 and phase ϕ of the pulse.

Constraints on the optimization are incorporated into the formalism using the technique of Lagrange multipliers (see for example, [26]), with a multiplier λ_i for each constraint. The vector Bloch equation thus introduces a vector Lagrange multiplier $\boldsymbol{\lambda}$. Some suitable measure of pulse performance, the cost function Φ, is then defined as the object of the optimization. One then finds that $\boldsymbol{\lambda}$ must also obey the Bloch equation at each time for the cost to be optimized, with its value at the end of the interval given by $\boldsymbol{\lambda}(t_p) = \partial\Phi/\partial\boldsymbol{M}$.

2.1.1. Application to phase modulation

Since optimal control theory is a generalization (e.g., [21]) of the classical Euler–Lagrange formalism, a "hamiltonian" h can be defined in terms of $\boldsymbol{\lambda}$ and the constraints on the possible trajectories as

$$h = \boldsymbol{\lambda}\cdot(\boldsymbol{\omega}_e \times \boldsymbol{M}) = \boldsymbol{\omega}_e \cdot (\boldsymbol{M} \times \boldsymbol{\lambda}). \tag{3}$$

In terms of general controls u_i, the final conditions that are necessary for the cost to be optimal are that

$$\frac{\partial h}{\partial u_i} = 0 \tag{4}$$

at all times throughout the evolution. If Eq. (4) is not equal to zero, it represents a gradient giving the proportional adjustment to make in the controls for a more optimal solution.

In our previous work, the controls were equal to $\boldsymbol{\omega}_e$, giving $\partial h/\partial\boldsymbol{\omega}_e = \boldsymbol{M}\times\boldsymbol{\lambda}$. As noted in the previous section, since very few spectrometers implement frequency modulation directly, the controls were restricted to the transverse, (x, y), components represented by $\boldsymbol{\omega}_{\mathrm{rf}}$ in Eq. (2). The z component of $\boldsymbol{M}\times\boldsymbol{\lambda}$ was therefore irrelevant in adjusting the controls.

For a constant amplitude phase-modulated pulse, ω_1 in Eq. (2) is time-independent and the only control is the phase, ϕ. Plugging $\boldsymbol{\omega}_e$ from Eq. (2) into Eq. (3) and setting $\partial h/\partial\phi = 0$ gives, together with the previous conditions on the evolution of $\boldsymbol{M}$ and $\boldsymbol{\lambda}$, the following requirements to optimize the cost:

$$\dot{\boldsymbol{M}} = \boldsymbol{\omega}_e \times \boldsymbol{M}, \qquad \boldsymbol{M}(t_0) = \hat{\boldsymbol{z}} \tag{5}$$

$$\dot{\boldsymbol{\lambda}} = \boldsymbol{\omega}_e \times \boldsymbol{\lambda}, \qquad \boldsymbol{\lambda}(t_p) = \partial\Phi/\partial\boldsymbol{M} \tag{6}$$

$$\boldsymbol{\omega}_{\mathrm{rf}} \cdot (\boldsymbol{\lambda}M_z - \boldsymbol{M}\lambda_z) = 0. \tag{7}$$

2.1.2. The cost function

The dot product $\Phi = \boldsymbol{M}(t_p)\cdot\boldsymbol{F}$ is one possible choice for quantifying the degree to which $\boldsymbol{M}(t_p) = \boldsymbol{F}$, which gives $\boldsymbol{\lambda}(t_p) = \boldsymbol{F}$ from Eq. (6) [14–16]. For alternative cost functions see Ref. [17]. For any of the cost functions, the procedure is the same–$\boldsymbol{M}$ and $\boldsymbol{\lambda}$ obey the Bloch equation,

and they can be calculated at each time for a given pulse. $\boldsymbol{M}_{\mathrm{opt}}(t)$ will satisfy the stationary condition of Eq. (7) when $\boldsymbol{\lambda}_{\mathrm{opt}}(t) = 0$. For a non-optimal pulse, the gradient calculated in Eq. (7) for each time point of the two trajectories gives the proportional adjustment to make in the pulse phase ϕ.

2.2. Numerical algorithm

The procedure for optimizing the cost can be incorporated in the following algorithm:

(i) Choose an initial RF sequence $\boldsymbol{\omega}_e^{(0)}$.
(ii) Evolve $\boldsymbol{M}$ forward in time from the initial state $\hat{\boldsymbol{z}}$.
(iii) Evolve $\boldsymbol{\lambda}$ backward in time from the target state $\hat{\boldsymbol{x}}$.
(iv) $\phi^{(k+1)}(t) \rightarrow \phi^{(k)}(t) + \epsilon \boldsymbol{\omega}_{\mathrm{rf}} \cdot (\boldsymbol{\lambda} M_z - \boldsymbol{M} \lambda_z)$.
(v) Repeat steps (ii)–(iv) until a desired convergence of Φ is reached.

Since the optimization is performed over a range of chemical-shift offsets and variations in the peak RF calibration, the gradient used in step (iv) is averaged over the entire range. Additional details of the averaging procedure and the choice of stepsize ϵ for incrementing the phase in each iteration are described in [14,15].

3. Results and discussion

In our work to date, we have focused on demonstrating the capabilities of optimal control theory for NMR pulse design, establishing the effectiveness of the algorithms and the viability of the resulting pulses. The excitation pulse is a simple example that characterizes optimal control behavior in NMR while minimizing its convolution with any particular application. This characterization establishes a foundation for pursuing other applications. We first assess the performance of the calibration-free phase-modulated pulse derived by the new algorithm, then consider applications to two commonly used pulse sequences, illustrating the advantages of the new pulse.

3.1. Pulse performance

Pulse performance, in general, depends on the pulse duration, with pulses of sufficient length giving the optimal control algorithm the flexibility to obtain practically ideal results in many cases. In addition, excitation (and inversion) efficiency undergoes a steep drop in performance below a minimum pulse length [16], which depends on the parameters defining the optimization. Increasing pulse length significantly above this minimum provides only marginal improvement, so the shortest pulse that provides acceptable performance is the goal.

Choosing 2 ms for the pulse length initially and optimizing with the new algorithm provided a pulse that transforms 99.9% of initial z magnetization to within 1.5° of the x-axis over a resonance offset range of 50 kHz for a constant RF amplitude anywhere in the range 10–20 kHz (results not shown). This nearly ideal performance can be traded for shorter pulse length. Since performance drops rapidly for shorter pulses, we find that overdigitizing the initial waveform used in the optimal control procedure gives the algorithm additional flexibility in finding the best solution, as discussed in Ref. [17]. Every other point of the resulting pulse is used as the initial input for generating a new pulse, and this procedure is continued until a minimal digitization with acceptable performance is reached. For a 1 ms pulse length, 320,000 random phases were input initially (~3 ns per time step). Such a large number of parameters would be extremely difficult, if not impossible, to optimize using conventional methods. This "breeder" pulse resulted in the final 625-point pulse shown in Fig. 1.

3.1.1. Comparison to existing pulses

Although adiabatic pulses accommodate a wide range of peak power levels, the exceptional bandwidth of adiabatic inversion for a given peak RF amplitude does not translate to excitation. The orientation of the effective RF field at the end of an adiabatic excitation pulse, which, ideally gives the location of the magnetization, is not in the transverse plane for non-zero chemical-shift offset. Other existing

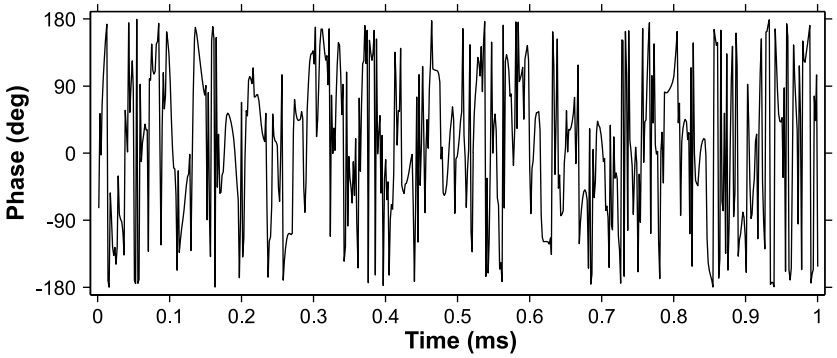

Fig. 1. Phase modulation of the constant amplitude 1 ms PM-BEBOP pulse. This pulse performs the point-to-point transformation $I_z \rightarrow I_x$ over a 50 kHz range of resonance offsets for constant RF amplitude set anywhere in the range 10–20 kHz (see Figs. 2 and 3).

excitation pulses [1–13] provide only limited dual compensation for RF variability and resonance offset. Moreover, they have not demonstrated a performance advantage over phase-compensated hard pulses, so hard 90° pulses could be considered the benchmark for broadband performance in sequences that are readily phase-corrected.

The theoretical performance of the optimized pulse and of a conventional hard pulse are illustrated in Fig. 2. Contours of resulting x magnetization, M_x, are plotted as functions of resonance offset and RF amplitude of the pulses (Figs. 2A and C). Similarly, the contours of magnetization in the transverse plane, $\sqrt{M_x^2+M_y^2}$, are shown for the hard pulse in comparison (Fig. 2B). The M_x magnetization excited by a hard pulse is strongly dependent on offset, with a narrow bandwidth of approximately ±2.5 kHz for greater than 99% excitation, using a calibrated RF amplitude of 15 kHz (Fig. 2A). In most applications, however, excitation pulses are used around evolution periods, in which case phase deviations can be compensated by a first order phase correction. Hence, the excitation profile of transverse magnetization, $\sqrt{M_x^2+M_y^2}$, is more appropriate for a comparison, resulting in a bandwidth of ±12.5 kHz with larger than 99% excitation for a calibrated 15 kHz hard pulse (Fig. 2B).

Regardless of the application, hard excitation pulses are significantly affected by RF miscalibrations. On resonance, where the performance is best, only 90% of magnitization is brought into the transverse plane if the pulse amplitude deviates by 25% from its nominal value. For the optimized phase-modulated BEBOP (PM-BEBOP) pulse of 1 ms duration, the excited magnetization M_x is better than 99% of the initial z magnetization, M_0, over the targetted factor of two variation in the nominal RF delivered by the coil and resonance offsets of ±25 kHz, as shown in Fig. 2C. Phase deviations over the optimization window are typically less than 2–3° (cf. Fig. 3), which is sufficient for the majority of NMR-experiments. In applications with a high dynamic range, as for example in ^{1}H-NOESY experiments, this phase behavior might not be adequate. In such cases, pulses with more stingently optimized phase behavior (and shorter pulse length) can be used [15,17], with the proviso that they also require more accurate calibration.

Experimental excitation profiles were implemented on Bruker Avance spectrometers equipped with SGU units for RF control and linearized amplifiers. For testing the performance of the phase modulated BEBOP pulses, a sample of 99.96 % D_2O was doped with $CuSO_4$ to a final T_1 relaxation time of ~500 ms. To reduce effects of B_1-field inhomogeneity, approximately 40 µl of this solution was placed in a Shigemi limited volume tube. The maximum RF amplitude was calibrated using a square shaped pulse. Offset profiles were then obtained by varying the offset of the shaped pulses from −27 kHz to 27 kHz in steps of 1 kHz. To also monitor the B_1-field dependence of the pulses, the experiments were repeated with ±1, ±2, and ±3 dB attenuation relative to a central RF amplitude,

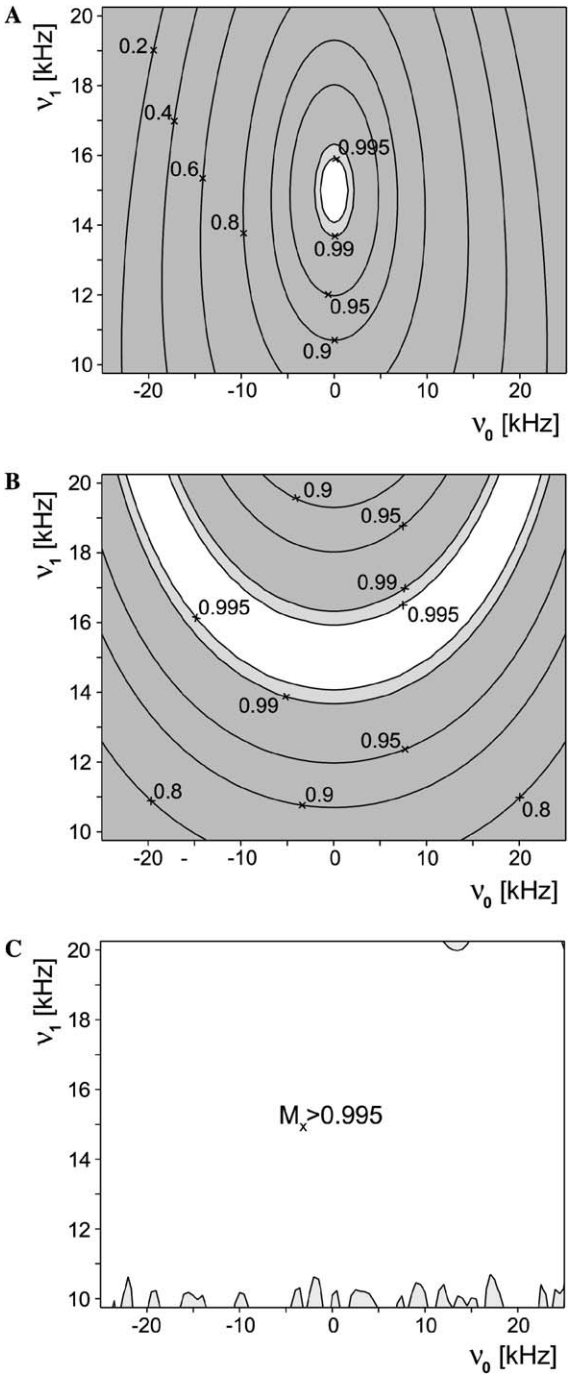

Fig. 2. Simulated performance of (A and B) a hard excitation pulse and (C) the optimized PM-BEBOP pulse of Fig. 1 plotted as a function of RF amplitude ν_1 and resonance offset ν_0. The nominal RF amplitude is 15 kHz. Theoretical transfer from initial z magnetization M_0 to (A and C) M_x and (B) the transverse plane $\sqrt{M_x^2+M_y^2}$ is shown. White areas correspond to transfers larger than 99.5%, light gray to transfer between 99.0 and 99.5% and darker gray to transfer below 99.0%. While transfer to M_x for the hard pulse has very limited bandwidth and tolerance to RF variation (A), the phase modulated BEBOP pulse shows almost perfect excitation over the whole offset and RF amplitude range shown. In readily phase-compensated pulse sequences the transfer of initial magnetization to the transverse plane is important, as shown in (B) for the hard pulse. The performance of the hard pulse in this case is strongly improved compared to its transfer properties to M_x, but there is significant loss per applied pulse for amplitudes lower than the nominal 15 kHz.

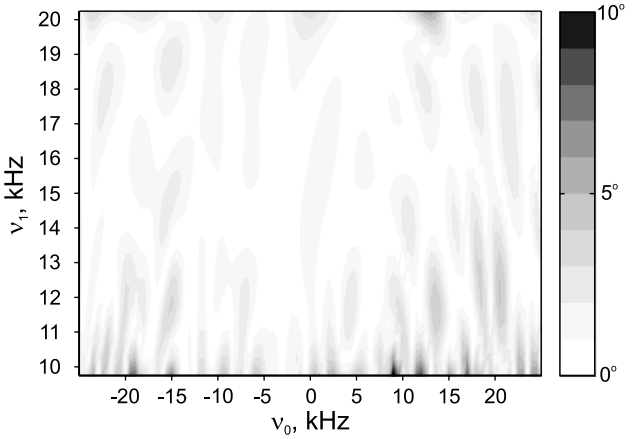

Fig. 3. The phase behavior of the optimized PM-BEBOP pulse of Fig. 1 is plotted as a function of RF amplitude ν_1 and resonance offset ν_0. Phase deviations from an ideal excitation pulse are shown in 1° steps in different shades of gray (see scale to the right). For almost the entire range of offsets and RF amplitudes, the phase is less than 2–3°, with minor distortions in the 6–9° range at the lowest RF (10 kHz) in the optimized range.

corresponding to RF amplitudes of 10.0, 11.2, 12.6, 14.1, 15.8, 17.8, and 20.0 kHz. The results are shown in Fig. 4. The experimental data provide an excellent match with theory and represent a considerable improvement over the maximum attainable performance of a phase-corrected hard pulse, opening the door to practically calibration-free excitation pulses.

3.2. 2D applications

The benefits of using PM-BEBOP in practical NMR applications are well-illustrated by ^{13}C–^{1}H correlated experiments, as e.g., HSQC or HMBC. An important element of these types of experiment is the sub-sequence 90°–t_1–90° applied to the ^{13}C spins to encode the frequencies for the first dimension of the 2D spectrum. The linear phase roll of a hard 90° pulse is commonly eliminated from the first spectral dimension by subtracting a constant time (equal to $4t_{90}/\pi$) from t_1. Details of the mechanism responsible for this "rephasing" are straightforward, but it suffices to note merely that one can expect approximately phase-corrected performance from hard 90° pulses in HSQC-type sequences, at least in the absence of RF inhomogeneity.

Two-dimensional spectra were recorded on a Bruker Avance 500 spectrometer using a ≈500 mM menthol sample dissolved in $CDCl_3$. Standard HSQC [28,29] and HMBC experiments [30,31] were acquired with variations in offset, RF amplitude, and the kind of pulses applied on ^{13}C nuclei. The maximum RF amplitude of the Bruker TXI probehead used corresponds to 14.3 kHz (equivalent to a 90° pulse of 17.5 μs). To avoid maximum power for the shaped pulses, we used slightly lower RF amplitudes of 12 kHz for the nominal power. This scales to a 1.2 ms PM-BEBOP pulse covering ±20 kHz bandwidth (rather than the 15 kHz nominal amplitude of the 1 ms pulse shown in Fig. 1, which has a bandwidth of ±25 kHz).

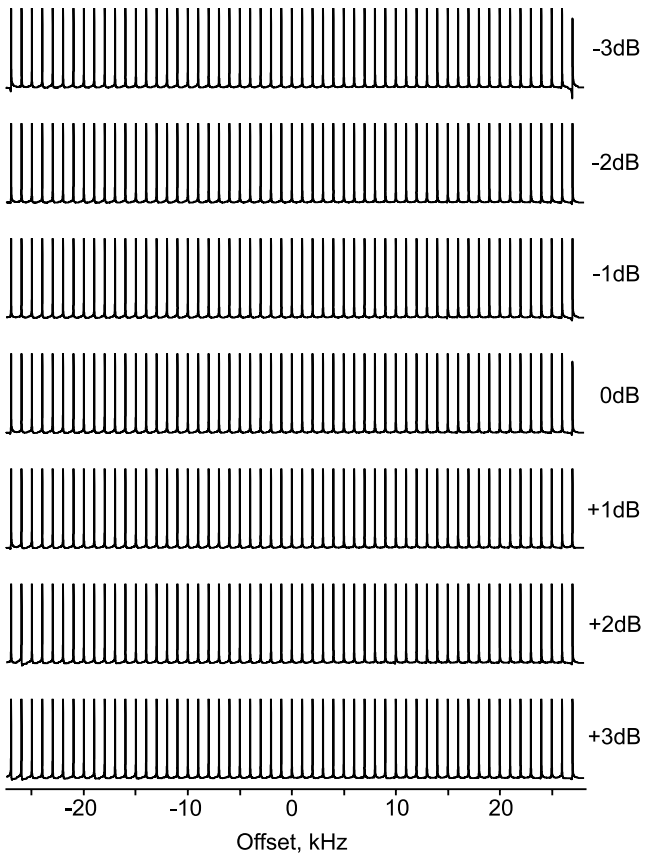

Fig. 4. Excitation profiles for the residual HDO signal in a sample of 99.96% D_2O are displayed as a function of resonance offset (1 kHz increments) and RF power levels applied using the 1 ms PM-BEBOP pulse of Fig. 1. The pulse was applied with constant amplitudes of 10 kHz (+3 dB), 11.2 kHz (+2 dB), 12.6 kHz (+1 dB), 14.1 kHz (0 dB), 15.8 kHz (−1 dB), 17.8 kHz (−2 dB), and 20 kHz (−3 dB). The experimental performance of the pulse is in excellent agreement with theory, producing practically perfect excitation, $M_x > 0.99M_0$, over ±25 kHz for RF variability within ±33.3% (∼6 dB) of the nominal value 15 kHz.

The total sweep width needed for covering the ^{13}C-spectra of menthol on a 500 MHz spectrometer is ≈8 kHz. We therefore, decided to record three spectra with 0, 8, and 16 kHz offset relative to the center of the ^{13}C-spectral width, leading to a coverage of offsets corresponding to −4–4, 4–12, and 12–20 kHz, respectively. Since spectral width and offsets are matched, no folding artefacts were observed.

Based on the procedure described in [27], we also constructed a 2.4 ms, 180° universal rotation pulse consisting of the original PM-BEBOP pulse appended to its phase and time-reversed version, resulting in a pulse with an active bandwidth identical to the pulse from which it originates. The performance of the resulting inversion/refocusing pulse with respect to offset and RF amplitude is shown in Fig. 5 in comparison to a hard 180° pulse. To test the robustness of the pulse sequences with respect to variation in RF amplitude, hard and shaped pulses were set to 8, 10, and 12 kHz RF amplitude.

For each combination of offset and RF amplitude, three HSQC and three HMBC experiments were acquired using

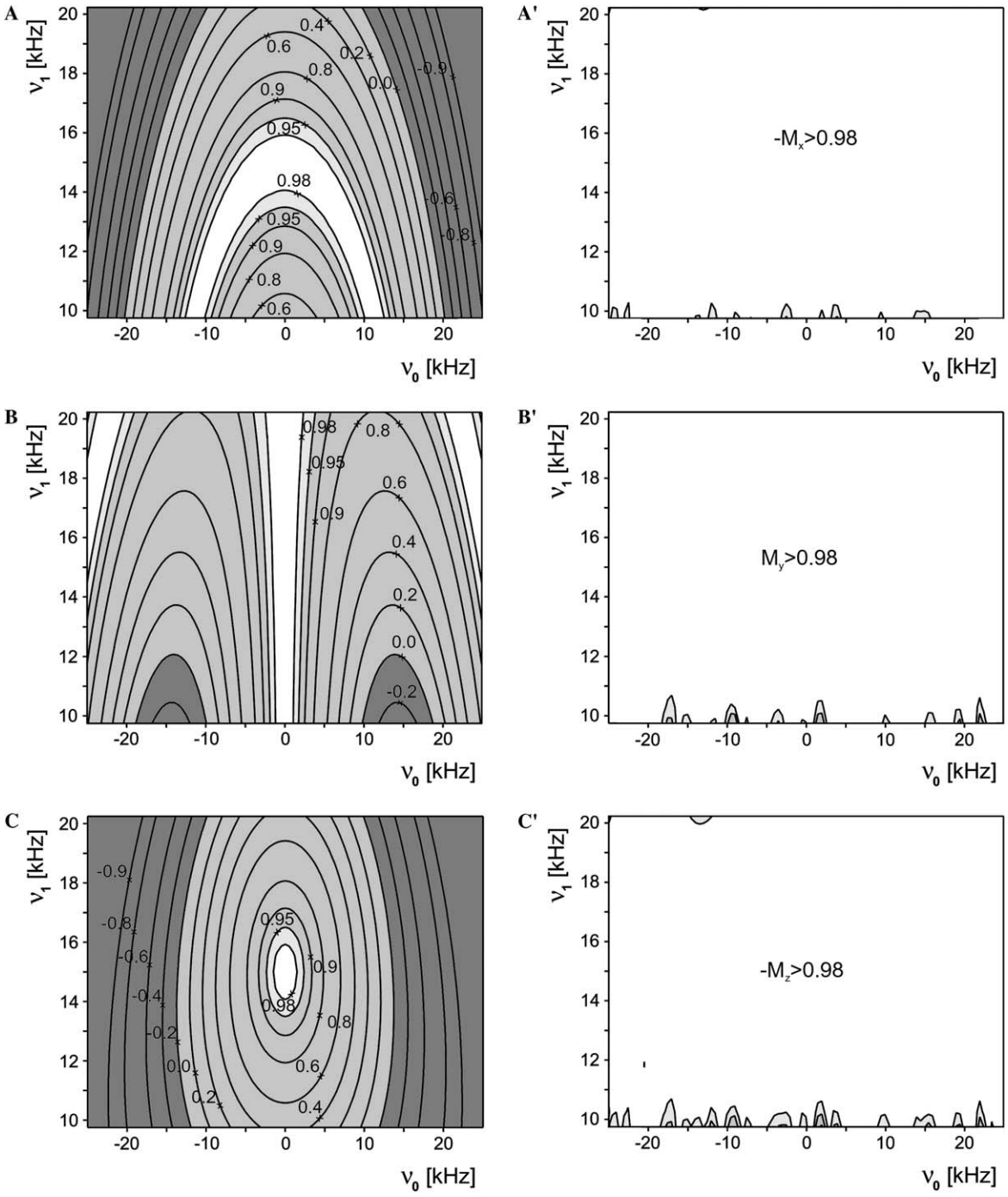

Fig. 5. Simulated refocusing performance is shown as a function of RF amplitude ν_1 and resonance offset ν_0 for a hard 180° pulse generating the transformations (A) $-M_x \rightarrow M_x$, (B) $M_y \rightarrow M_y$, and (C) $M_z \rightarrow -M_z$. The corresponding performance of a shaped 180° pulse constructed from the optimized PM-BEBOP pulse of Fig. 1 using the procedure described in [27] is shown in the second column of figures. The nominal RF amplitude is 15 kHz in all cases. White areas correspond to transfers larger than 98.0%, light gray to transfer between 95.0% and 98.0%, gray to lower positive transfer, and dark gray to transfer where the resulting magnetization is still negative. While refocusing for the hard pulse has very limited bandwidth and tolerance to RF variation, the pulse constructed from the PM-BEBOP pulse shows very good refocusing properties over the whole offset and RF amplitude range shown.

only hard pulses, hard excitation but shaped PM-BEBOP-based 180° pulses, and only shaped PM-BEBOP excitation and PM-BEBOP-based refocusing pulses, respectively, on ^{13}C nuclei (Fig. 6). In the series of experiments with shaped excitation pulses, the 90° flip back pulse after the ^{13}C evolution period was replaced by the time-reversed PM-BEBOP pulse for optimal transfer $M_x \rightarrow M_z$. In Figs. 7 and 8, representative slices of all 2D-spectra acquired through

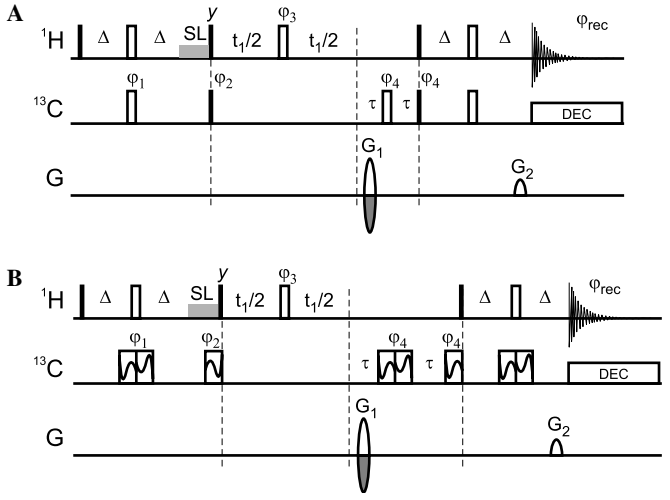

Fig. 6. HSQC pulse sequences used for the comparison of signal intensities shown in Fig. 7. The reference HSQC based on hard pulses is shown in (A). In the sequence shown in (B) all ^{13}C-pulses are replaced by PM-BEBOP-based excitation and refocusing pulses. PM-BEBOP pulses are schematically shown as rectangular pulses (representing constant RF amplitude) containing a wavy line (representing phase-modulation). Phase and/or time reversals are illustrated by vertical and/or horizontal mirroring of the wavy lines in the boxes, respectively. Phases are $\varphi_1 = x$, $\varphi_2 = x,-x$, $\varphi_3 = x,x,-x,-x$, $\varphi_4 = x,x,x,x,-x,-x,-x,-x$, $\varphi_{rec} = x,-x,x,-x,-x,x,-x,x$. G1, φ_1, φ_2, and φ_{rec} are cycled ± according to echo/antiecho acquisition scheme. If not stated otherwise, all pulses have x phase.

the signals corresponding to $C_6H_6^{eq}$ and C_1H_7, respectively, are shown. The slices taken from HMBC spectra are shown in magnitude mode.

On resonance and with correctly calibrated hard pulses, the performance of all three HSQC experiments is more or less identical (cf. Fig. 7A). However, as soon as either RF amplitude or resonance offsets are changed, the signal intensity of the hard pulse HSQC decreases substantially, and at offsets larger than 15 kHz the signal falls to ≈0 (cf. Fig. 7C–C″). In addition, large phase rolls are observed in the indirect dimension.

Most of the signal loss is due to the bad performance of the uncompensated hard 180° pulses. As expected from previous reports [12,32–34], replacing the hard inversion pulses with broadband refocusing pulses recovers most of the signal over the operating bandwidth of the pulse. The PM-BEBOP-based refocusing pulse provides the same bandwidth and tolerance to RF inhomogeneity or miscalibration as the excitation pulse used in its construction, so that for RF amplitudes 3.5 dB lower than the nominal value and an 8 kHz offset (cf. Fig. 7B″), the signal intensity is practically identical to the on resonance case with calibrated RF amplitude.

In comparison, it is difficult to find broadband adiabatic refocusing pulses that achieve the performance of the new pulse shown in Fig. 5. To work properly, they must be sufficiently adiabatic, which is determined by pulse length, peak RF, and the frequency sweep range of the pulse (related to bandwidth). Typical adiabatic pulse shapes require pulse lengths of 3–4 ms to refocus over a 20% smaller bandwidth and smaller range of RF tolerance. The best adiabatic refocusing we could find (matching the 98% refocusing of Fig. 5) was achieved with WURST–20 [35]. Using a 0.5 ms pulse with a 94 kHz frequency sweep as the constituent inversion pulse of the 3π procedure described in [12] resulted in a 2 ms refocusing pulse which covered the full 50 kHz bandwidth for peak RF in the range 11.5–22 kHz.

Nevertheless, for larger offsets and lower RF amplitudes the overall intensity of experiments is also affected by the decreased performance of hard excitation pulses. At an offset of 16 kHz and a 3.5 dB miscalibrated RF amplitude, for example, the signal intensity is reduced by about one third (Fig. 7C″). When all carbon pulses are replaced by PM-BEBOP excitation and refocusing pulses, the signal intensity is restored also in these cases and virtually identical performance for the HSQC experiment is observed for the whole range of offsets and RF amplitude settings shown in Fig. 7.

The set of experiments recorded for the state of the art HMBC basically lead to identical results with respect to signal intensities (cf. Fig. 8). PM-BEBOP pulses appear to have a utility for excitation and refocusing pulses similar to adiabatic pulses for RF-compensated inversion, with almost no variation in pulse performance over the targetted offset and RF amplitude ranges.

4. Conclusion

We have derived an optimal control algorithm for designing purely phase-modulated pulses. Compared to earlier BEBOP pulses, advantages include simplified implementation and improved practical performance, since the output fidelity of phase modulation does not depend on amplifiers with linear amplitude. We derived a 1 ms pulse capable of uniformly exciting the entire 200 ppm ^{13}C chemical-shift range of a potential 1 GHz spectrometer for a peak RF amplitude anywhere in the range 10–20 kHz. This provides an unprecedented combination of bandwidth and tolerance to RF inhomogeneity. For probes which have a peak RF in this range, which should cover the vast majority of probes, one needs only to set the RF slightly lower than the maximum power (typically 3 dB attenuation) to ensure complete excitation. This removes a significant obstacle to automated NMR, which has been the need to accurately calibrate the constituent RF pulses in complex 2D pulse sequences. As noted, adiabatic pulses are tolerant to a wide range of RF miscalibration only as an inversion pulse. HSQC and HMBC experiments were provided to show the practical benefits of the new pulse.

BEBOP and PM-BEBOP pulses obtained to date can be downloaded in Bruker and Varian formats from http://www.org.chemie.tu-muenchen.de/people/bulu/.

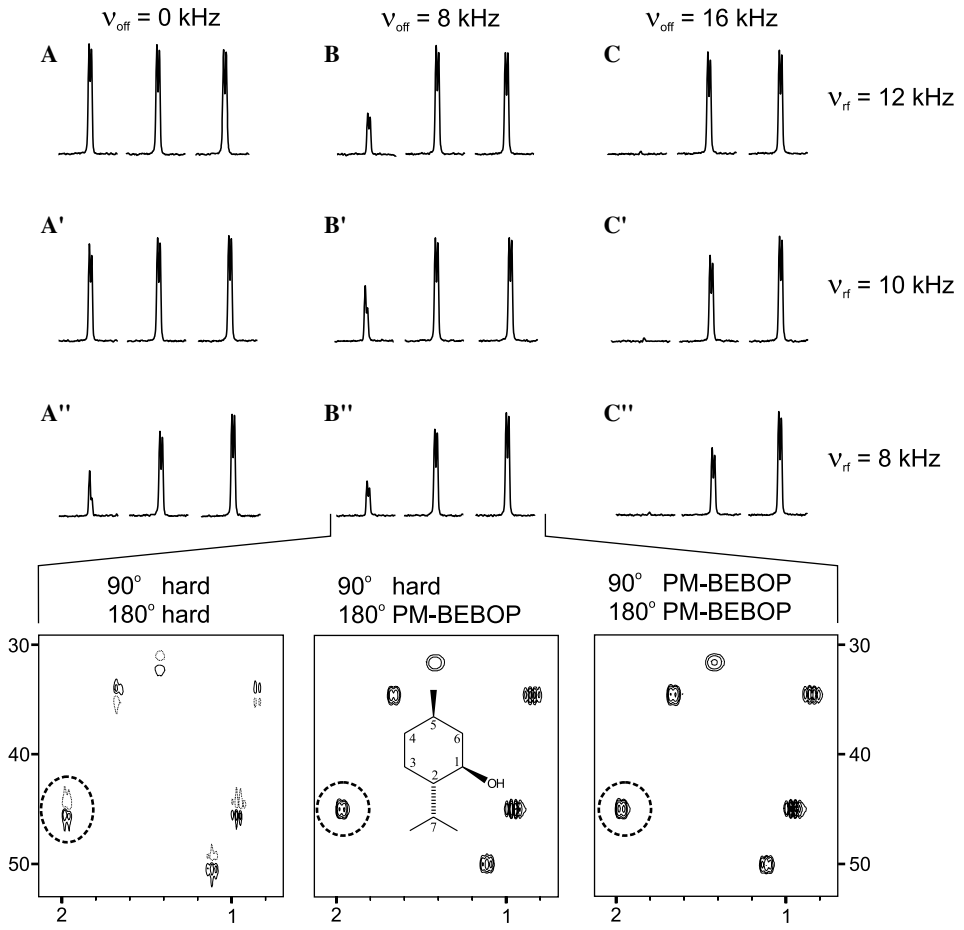

Fig. 7. Traces through the C_6-H_6^{eq} signal of several HSQC spectra of menthol in $CDCl_3$ recorded with various offsets, RF amplitudes, and ^{13}C pulses. RF amplitudes were 12 kHz (A,B,C), 10 kHz (A′, B′, C′), and 8 kHz (A″, B″, C″) and on-resonant offsets were set to 0 kHz (A–A″), 8 kHz (B–B″), and 16 kHz (C–C″) (see main text for details). For each offset and RF amplitude combination, the traces for three different HSQC experiments using different ^{13}C-pulses (see Fig. 6) are shown: only hard pulses (left), hard excitation and PM-BEBOP-based shaped 180° pulses (middle), and only PM-BEBOP excitation, and PM-BEBOP-based refocusing pulses (right). For B″, 2D-regions are also shown for the three different experiments for a better demonstration of the spectral quality. The circled signals correspond to the above traces. In the 2D-regions of spectra acquired using hard pulses, phase distortions can clearly be seen. These phase distortions have been corrected for all traces shown above in order to have a fair comparison of the intensities present in the various spectra.

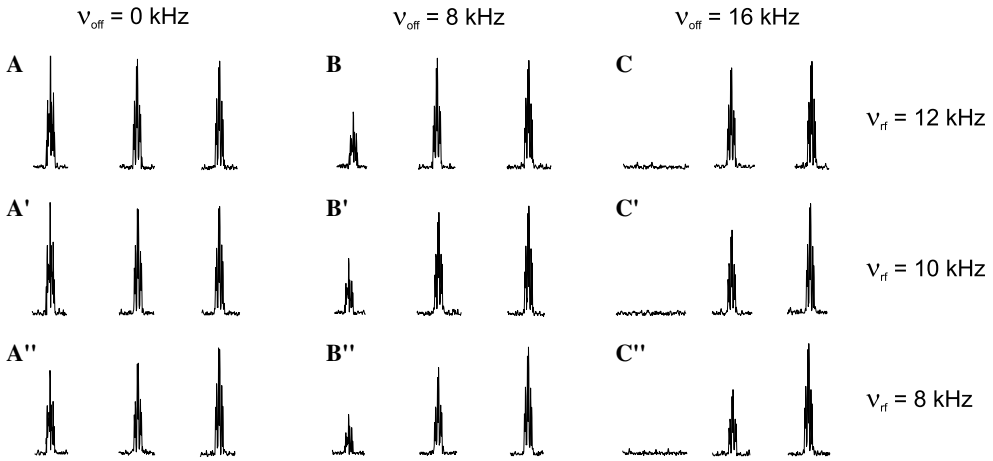

Fig. 8. Traces through the C_1-H_7 signal in HMBC spectra analogous to the traces of HSQC spectra shown in Fig. 7. The replacement of hard 180° pulses by the BEBOP-constructed 180° pulse significantly improves performance (see also [12,32–34]). Further improvements can be seen if both PM-BEBOP excitation and PM-BEBOP-based refocusing pulses are applied to ^{13}C: signal intensities basically stay constant for all RF amplitudes and offsets recorded.

Acknowledgments

T.E.S. acknowledges support from NSF Grant CHE-0518174. B.L. thanks the Fonds der Chemischen Industrie and the Deutsche Forschungsgemeinschaft (Emmy Noether fellowship LU 835/1-3) for support. S.J.G. acknowledges support from the Deutsche Forschungsgemeinschaft for Grant Gl 203/4-2 and the Fonds der Chemischen Industrie. N.K. acknowledges Darpa Grant F49620-0101-00556.

References

[1] R. Freeman, S.P. Kempsell, M.H. Levitt, Radiofrequency pulse sequences which compensate their own imperfections, J. Magn. Reson. 38 (1980) 453–479.
[2] M.H. Levitt, Symmetrical composite pulse sequences for NMR population inversion. I. Compensation of radiofrequency field inhomogeneity, J. Magn. Reson. 48 (1982) 234–264.
[3] M.H. Levitt, R.R. Ernst, Composite pulses constructed by a recursive expansion procedure, J. Magn. Reson. 55 (1983) 247–254.
[4] R. Tycko, H.M. Cho, E. Schneider, A. Pines, Composite pulses without phase distortion, J. Magn. Reson. 61 (1985) 90–101.
[5] M.H. Levitt, Composite pulses, Prog. Nucl. Magn. Reson. Spectrosc. 18 (1986) 61–122.
[6] A.J. Shaka, A.J. Pines, Symmetric phase-alternating composite pulses, J. Magn. Reson. 71 (1987) 495–503.
[7] J.-M. Böhlen, M. Rey, G. Bodenhausen, Refocusing with chirped pulses for broadband excitation without phase dispersion, J. Magn. Reson. 84 (1989) 191–197.
[8] J.-M. Böhlen, G. Bodenhausen, Experimental aspects of chirp NMR spectroscopy, J. Magn. Reson. Series A 102 (1993) 293–301.
[9] D. Abramovich, S. Vega, Derivation of broadband and narrowband excitation pulses using the Floquet Formalism, J. Magn. Reson. Series A 105 (1993) 30–48.
[10] Ē. Kupče, R. Freeman, Wideband excitation with polychromatic pulses, J. Magn. Reson. Series A 108 (1994) 268–273.
[11] K. Hallenga, G.M. Lippens, A constant-time ^{13}C–^{1}H HSQC with uniform excitation over the complete ^{13}C chemical shift range, J. Biomol. NMR 5 (1995) 59–66.
[12] T.L. Hwang, P.C.M. van Zijl, M. Garwood, Broadband adiabatic refocusing without phase distortion, J. Magn. Reson. 124 (1997) 250–254.
[13] K.E. Cano, M.A. Smith, A.J. Shaka, Adjustable, broadband, selective excitation with uniform phase, J. Magn. Reson. 155 (2002) 131–139.
[14] T.E. Skinner, T.O. Reiss, B. Luy, N. Khaneja, S.J. Glaser, Application of optimal control theory to the design of broadband excitation pulses for high resolution NMR, J. Magn. Reson. 163 (2003) 8–15.
[15] T.E. Skinner, T.O. Reiss, B. Luy, N. Khaneja, S.J. Glaser, Reducing the duration of broadband excitation pulses using optimal control with limited RF amplitude, J. Magn. Reson. 167 (2004) 68–74.
[16] K. Kobzar, T.E. Skinner, N. Khaneja, S.J. Glaser, B. Luy, Exploring the limits of broadband excitation and inversion pulses, J. Magn. Reson. 170 (2004) 236–243.
[17] T.E. Skinner, T.O. Reiss, B. Luy, N. Khaneja, S.J. Glaser, Tailoring the optimal control cost function to a desired output: application to minimizing phase errors in short broadband excitation pulses, J. Magn. Reson. 172 (2005) 17–23.
[18] L. Pontryagin, B. Boltyanskii, R. Gamkrelidze, E. Mishchenko, The Mathematical Theory of Optimal Processes, Wiley-Interscience, New York, 1962.
[19] A.P. Sage, Optimum Systems Control, Prentice-Hall, Inc., Englewood Cliffs, NJ, 1968.
[20] A. Bryson Jr., Y.-C. Ho, Applied Optimal Control, Hemisphere, Washington, D.C., 1975.
[21] E. Pinch, Optimal Control and the Calculus of Variations, Oxford University Press, Oxford, 1993.
[22] S. Conolly, D. Nishimura, A. Macovski, Optimal control solutions to the magnetic resonance selective excitation problem, IEEE Trans. Med. Imaging MI-5 (1986) 106–115.
[23] J. Mao, T.H. Mareci, K.N. Scott, E.R. Andrew, Selective inversion radiofrequency pulses by optimal control, J. Magn. Reson. 70 (1986) 310–318.
[24] D. Rosenfeld, Y. Zur, Design of adiabatic selective pulses using optimal control theory, Magn. Reson. Med. 36 (1996) 401–409.
[25] N. Khaneja, T. Reiss, C. Kehlet, T. Schulte-Herbrüggen, S.J. Glaser, Optimal Control of Coupled Spin Dynamics: Design of NMR Pulse Sequences by Gradient Ascent Algorithms, J. Magn. Reson. 172 (2005) 296–305.
[26] H. Goldstein, Classical Mechanics, Addison-Wesley, Reading, MA, 1980.
[27] B. Luy, K. Kobzar, T.E. Skinner, N. Khaneja, S.J. Glaser, Construction of Universal Rotations from Point to Point Transformations, J. Magn. Reson. 176 (2005) 179–186.
[28] G. Bodenhausen, D.J. Ruben, Natural abundance N-15 NMR by enhanced heteronuclear spectroscopy, Chem. Phys. Lett. 69 (1980) 185–189.
[29] A.L. Davis, J. Keeler, E.D. Laue, D. Moskau, Experiments for recording pure-absorption heteronuclear correlation spectra using pulsed field gradients, J. Magn. Reson. 98 (1992) 207–216.
[30] A. Bax, M.F. Summers, H-1 and C-13 assignments from sensitivity-enhanced detection of heteronuclear multiple-bond connectivity by 2D multiple quantum NMR, J. Am. Chem. Soc. 108 (1986) 2093–2094.
[31] L. Verdier, P. Sakhaii, M. Zweckstetter, C. Griesinger, Measurement of long-range H,C couplings in natural products in orienting media: a tool for structure elucidation of natural products, J. Magn. Reson. 163 (2004) 353–359.
[32] K. Hallenga, G.M. Lippens, A constant-time C-13-H-1 HSQC with uniform excitation over the complete C-13 chemical-shift range, J. Biomol. NMR 5 (1995) 59–66.
[33] P.C.M. van Zijl, T.L. Hwang, M. O'Neil Johnson, M. Garwood, Optimized excitation and automation for high-resolution NMR using B-1-insensitive rotation pulses, J. Am. Chem. Soc. 118 (1996) 5510–5511.
[34] K. Ogura, H. Terasawa, F. Inagaki, Fully C-13-refocused multidimensional C-13-edited pulse schemes using broadband shaped inversion and refocusing pulses, J. Magn. Reson. Series B 112 (1996) 63–68.
[35] Ē. Kupče, R. Freeman, J. Magn. Reson. Series A 115 (1995) 273–276.